Adaptive mesh refinements for analyses of 2D linear elasticity problems using the Kriging-based finite element method

Johanna Handoko[1*], *Foek Tjong* Wong[1]

[1]Civil Engineering Department, Faculty of Civil Engineering and Planning, Petra Christian University, Jl. Siwalankerto 121-131, Surabaya 60236, Indonesia

Abstract. Finite element analyses of irregular structures require adaptive mesh refinement to achieve more accurate results in an efficient manner. This is also true for a non-conventional finite element method with Kriging interpolation, called the Kriging-based finite element method (K-FEM). This paper presents a study of automatic adaptive meshing procedures for analyses of two-dimensional linear elasticity problems using the K-FEM. The Matlab Partial Differential Equation Toolbox was utilized for generating meshes with Delaunay triangulation. Three error indicators, namely, the strain energy error, the gradient of effective stresses, and the element-free Galerkin strain energy error, were employed for estimating the element errors. To find the most effective error indicator, the resulting total number of elements and configurations of the final meshes were compared. The results show that the resulting final meshes were affected by the initial mesh configurations, the refinement criteria, and the termination criteria. The gradient of effective stresses indicator was found to be the most effective error indicator for the K-FEM, as it can accurately estimate the element errors.

1 Introduction

The mesh configurations used for finite element analyses of irregular structures must be properly considered. To predict the stresses more accurately, finer meshes are needed on some regions of the structures, such as the regions near holes and re-entrant corners. A uniform mesh refinement, however, results in a large number of elements and a long computational time. Hence, an automatic and adaptive mesh refinement (AMR) procedure, can be chosen to get more accurate results in an efficient manner. The AMR procedure is divided into two stages [1]. Firstly, the element errors are estimated using a selected error indicator. Secondly, after estimating the element errors, the mesh refinement is then carried out according to the element errors.

There are several error indicators available in literature. The strain energy error indicator [2-3] is based on the difference between unaveraged and averaged (smoothed) stresses. The gradient of effective stresses error indicator [4-5] was first implemented for the finite element analysis of shell elements. Based on the value of Von Mises stresses, this error indicator can identify the region with high-stress gradients. The gradient of effective stresses error indicator has been implemented by Pudjisuryadi [6] in the framework of the meshless local Petrov-Galerkin method. The element-free Galerkin strain energy error indicator [1, 7] is based on the difference between the computed and reference strain energy. The computed and reference strain energy are evaluated on a different number of Gauss points. In addition, the super-convergent patch recovery [8-12] is another type of error indicator that can be used.

The mesh refinement can be done by either *h*-refinement, *p*-refinement, or a combination of the *h*- and *p*-refinement [13]. The *h*-refinement will change the element size by doing an element subdivision or a complete remeshing. On the other hand, the polynomial order of an element will be changed through *p*-refinement.

An alternative method for the classical finite element method (FEM) to obtain more accurate analysis results is the Kriging-based finite element method (K-FEM) [14-17]. In the K-FEM, Kriging interpolation (KI) is employed as the trial and test functions. The KI is constructed not only using the element nodes but also the satellite nodes surrounding the element. Consequently, the domain of influence (DOI) of a node can be formed by layers of elements. Thus, the K-FEM is known as FEM with element-free shape functions. In comparison to the classical FEM, more accurate results can be achieved by the K-FEM with fewer elements by simply increasing the layers. An AMR procedure for the K-FEM has been studied by Masood [18] using the Galerkin local residual error estimator.

This paper presents a study of three AMR procedures for analyses of two-dimensional linear elasticity problems using the K-FEM. The problems considered are two benchmark problems of plane elasticity models, that is, a hollow cylinder and an infinite plate with a central hole [19]. The Matlab Partial Differential Equation (PDE) Toolbox [20] was used for

*Corresponding author: joannazz1707@gmail.com

generating meshes automatically with Delaunay triangulation and for performing adaptive meshing using the *h*-refinement. Moreover, the element errors were estimated by the three different error indicators, namely, the strain energy error [2-3], the gradient of effective stresses [4-6], and the element-free Galerkin strain energy error [1, 7]. The results in terms of the total number of elements and the final mesh configurations were then compared to find the most effective error indicator.

2 Error indicators and adaptive mesh refinement (AMR) strategies

2.1 Strain energy error (SER)

The SER error indicator [2-3] is based on the difference between the element unaveraged and averaged (smoothed) stress fields. The finite element unaveraged stress field is discontinuous on the element boundaries between neighboring elements. However, the element averaged stress field, constructed from averaged stresses at the element nodes, is continuous.

To obtain the SER, nodal averaged stresses in a DOI under consideration are first defined by Equations 1-2.

$$(\boldsymbol{\sigma}_{\text{ave}})_j = \frac{1}{a}\sum_{e=1}^{a} \boldsymbol{\sigma}_j^e \tag{1}$$

where:
$(\boldsymbol{\sigma}_{\text{ave}})_j$: nodal averaged stress vector at node j
a : number of elements surrounding node j
$\boldsymbol{\sigma}_j^e$: element unaveraged stress vector at node j, viz.

$$\boldsymbol{\sigma}_j^e = \langle \sigma_{xj}^e \quad \sigma_{yj}^e \quad \gamma_{xyj}^e \rangle \tag{2}$$

Afterward, the element smoothed stress field is constructed by interpolating the average stresses at the nodes in the DOI using the finite element shape functions by Equation 3.

$$\overline{\boldsymbol{\sigma}}^e = \sum_{j=1}^{n} N_j (\boldsymbol{\sigma}_{\text{ave}})_j \tag{3}$$

where:
$\overline{\boldsymbol{\sigma}}^e$: element averaged (smoothed) stress field
N_j : shape function associated with node j
n : number of nodes in the domain of influencing nodes

The element stress and strain energy error can then be calculated using the following Equations 4-5.

$$\boldsymbol{\sigma}_{\text{Er}}^e = \boldsymbol{\sigma}^e - \overline{\boldsymbol{\sigma}}^e \tag{4}$$

$$U_{\text{Er}} = \int_V \frac{1}{2} \boldsymbol{\sigma}_{\text{Er}}^{e\text{T}} \mathbf{E}^{-1} \boldsymbol{\sigma}_{\text{Er}}^e \, dV \tag{5}$$

where:
$\boldsymbol{\sigma}_{\text{Er}}^e$: vector of element stress error
U_{Er} : element strain energy error
$\mathbf{E}$: elasticity matrix

2.2 Gradient of effective stresses (GES)

The GES error indicator [4-6] can detect regions with high-stress gradients. These regions are identified by high-stress error values. A triangular element K (shaded area) with a central point P_K is shown in Fig.1. The element is surrounded by other elements with one side in common with element K. Each surrounding element has a central node P_{Ki}. The gradient of the effective stress is calculated by comparing the value of effective stresses at P_K to each P_{Ki}.

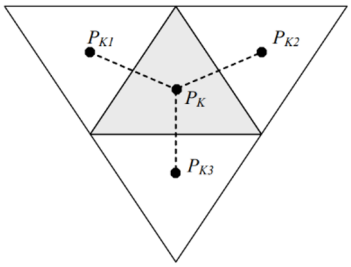

Fig. 1. A triangular element ***K*** (shaded area) [6].

The GES error indicator (E_K) can be defined using the following Equations 6-8.

$$E_K = h_K g_K \tag{6}$$

$$g_K = \max \frac{|\sigma_e(P_K) - \sigma_e(P_{Ki})|}{d(P_K, P_{Ki})} \tag{7}$$

$$\sigma_e(P_K) = \frac{1}{\sqrt{2}} \left[\begin{matrix} (\sigma_x - \sigma_y)^2 + (\sigma_y - \sigma_z)^2 + \\ (\sigma_z - \sigma_x)^2 + 6(\tau_{xy}^2 + \tau_{yz}^2 + \tau_{zx}^2) \end{matrix} \right]^{\frac{1}{2}} \tag{8}$$

where:
h_K : the smallest side length of a triangular element K
g_K : maximum gradient of effective stress at P_K
$\sigma_e(P_K)$: Von Mises stress at P_K
$d(P_K, P_{Ki})$: the distance from P_K to P_{Ki}

2.3 Element-free Galerkin (EFG) strain energy error

The EFG strain energy error [1, 7] was first implemented for the AMR procedure of meshless methods. The element strain energy error is defined as the difference between the computed and the reference strain energy. The computed strain energy (U_{comp}) is calculated using m_g number of Gauss points. On the other hand, the reference strain energy (U_{ref}) is calculated using n_g number of Gauss points (n_g<m_g). These can be seen in the following Equations 9-10.

$$U_{\text{comp}} = \sum_{g=1}^{m_g} c_g \boldsymbol{\sigma}_g{}^{e\text{T}} \boldsymbol{\varepsilon}_g{}^e \tag{9}$$

$$U_{\text{ref}} = \sum_{l=1}^{n_g} c_l \boldsymbol{\sigma}_l{}^{e\text{T}} \boldsymbol{\varepsilon}_l{}^e \tag{10}$$

where c_g and c_l are the corresponding integration weights of Gauss points.

The element strain energy error can then be calculated using the following Equation 11.

$$U_{\mathrm{Er}} = \left|U_{\mathrm{comp}} - U_{\mathrm{ref}}\right| \tag{11}$$

2.4 Refinement criteria

In this research, the criterion for selecting the elements to be refined was based on Equations 12-14 [4]:

$$\bar{e}^{\varepsilon_{\mathrm{ps}}} = \frac{1}{\mathrm{Numel}}\left[\sum_{K=1}^{\mathrm{Numel}} e_K^{\varepsilon_{\mathrm{ps}}}\right] \tag{12}$$

$$\xi_K = \frac{e_K^{\varepsilon_{\mathrm{ps}}}}{\bar{e}^{\varepsilon_{\mathrm{ps}}}} \tag{13}$$

$$\xi_K - 1 > \beta_{\varepsilon,\mathrm{tol}} \tag{14}$$

where:
$\bar{e}^{\varepsilon_{\mathrm{ps}}}$: average error of elements in the whole domain
Numel : total number of elements
$e_K^{\varepsilon_{\mathrm{ps}}}$: element error
$\beta_{\varepsilon,\mathrm{tol}}$: tolerance level

Based on the definition described above, an element will be refined if the error is larger than the average error with a particular level of tolerance ($\beta_{\varepsilon,\mathrm{tol}}$). In this research, the value of $\beta_{\varepsilon,\mathrm{tol}}$ was used as the input of the program. For determining this value, firstly, the authors tried to run the K-FEM analysis for a linear polynomial basis function with one layer of elements. Subsequently, the range of $\beta_{\varepsilon,\mathrm{tol}}$ was chosen by considering the relative strain energy error (RSER) in the first iteration. The value of $\beta_{\varepsilon,\mathrm{tol}}$ tended to be lowered as the value of RSER increased. A high value of RSER shows a less level of accuracy. By lowering the value of $\beta_{\varepsilon,\mathrm{tol}}$, more elements would be refined, and a better level of accuracy might be achieved. However, a low value of $\beta_{\varepsilon,\mathrm{tol}}$ could also result in an ineffective total number of elements and a distributed refinement process. Thus, the total number of elements and the final mesh configurations should also be considered for choosing the value of $\beta_{\varepsilon,\mathrm{tol}}$. In this research, the range of $\beta_{\varepsilon,\mathrm{tol}}$ was between 0.25 and 0.55, as these values could result in an effective total number of elements and final mesh configurations.

2.5 Relative strain energy difference (RSED)

In this research, the limit of RSED was used as the termination criteria of the AMR strategy. Therefore, the analysis would stop only when the RSED of the current iteration was already below the limit of the RSED chosen. This criterion is calculated using the difference between the total strain energy of the current iteration (U_k) and the previous iteration (U_{k-1}) by Equation 15 [21].

$$\mathrm{RSED} = \frac{|U_k - U_{k-1}|}{U_k} \tag{15}$$

The limit of RSED is chosen based on the user's desired level of accuracy. However, the limit of RSED should be lower than the value of RSED between the first and second iterations. Moreover, it is recommended to choose a limit lower than 5% (0.05). This is because a low limit of RSED indicates a more stable value of total strain energy. The total number of elements and the final mesh configurations should also be considered for choosing the suitable limit of RSED. Based on these criteria, in this research, the limit of RSED was taken from 0.003 to 0.05.

2.6 Relative strain energy error (RSER)

The RSER is defined as the difference between the exact or reference (U_{ex}) and K-FEM ($U_{\mathrm{K-FEM}}$) total strain energy (Equation 16). For problems without exact solutions, the reference total strain energy is calculated by running the K-FEM analysis for a cubic polynomial basis with three layers of elements using very fine meshes.

$$\mathrm{RSER} = \frac{|U_{\mathrm{ex}} - U_{\mathrm{K-FEM}}|}{U_{\mathrm{ex}}} \tag{16}$$

In this research, the RSER was only used as a checking criterion to evaluate whether the value of $\beta_{\varepsilon,\mathrm{tol}}$ was suitable or not. Therefore, the AMR procedure could still be done without the exact solution.

2.7 Matlab Partial Differential Equation (PDE) Toolbox

The Matlab PDE Toolbox can be used to solve many problems, such as plane stress, plane strain, electrostatic, magnetostatic, heat transfer, and diffusion [20]. Using a graphical user interface provided by the PDE Toolbox, the user can easily draw the geometry of the problem being analyzed. Furthermore, this toolbox can be used for generating unstructured meshes using Delaunay triangulation and performing the AMR using the element subdivision *h*-refinement. The data of the unstructured meshes generated from the PDE Toolbox, namely, the point, edge, triangle, geometry, and boundary condition matrices, can then be exported to the main workspace. These mesh data are used as the inputs of the AMR K-FEM program.

In this research, the AMR procedure was carried out using the three error indicators described above. The formulation of the error indicator in the PDE Toolbox AMR function (*adaptmesh*) was then modified into those three error indicators. Moreover, the refinement criterion was also modified. Furthermore, the longest edge refinement was chosen as the refinement method. By choosing this method, the AMR procedure would be done by bisecting the longest edge of selected triangles and introducing new nodes on the divided edges. Thus, the point and triangle matrices would be updated. In addition, the divided edge entries in the edge matrix would also be updated by two new entries. Fig. 2 shows the *h*-refinement procedure using the longest edge refinement around elements that do not pass the refinement criteria.

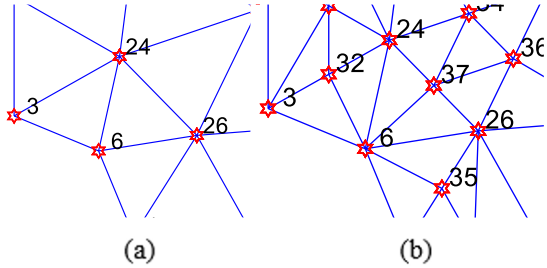

Fig. 2. The a) initial and b) final stages of the *h*-refinement procedure with the longest edge refinement.

3 Kriging interpolation (KI)

The Kriging interpolation (KI) of an element is constructed on the basis of nodes comprising layers of elements [14-17]. This concept can be seen in Fig. 3. Fig. 3 shows the domain of influencing nodes of an element that consists of one, two, and three layers of elements. The global field variable can then be obtained by combining the KI of all elements in the domain.

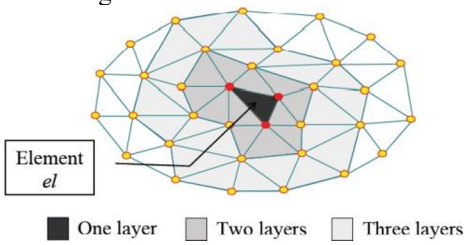

Fig. 3. Domain of influencing nodes of the element el [15].

The KI possesses the Kronecker delta and consistency properties [14-17, 22], which are important in the implementation of FEM. Furthermore, the K-FEM and the conventional FEM use a similar computational procedure. Therefore, a conventional FEM program can be easily modified to include the K-FEM concept.

In this section, the formulation of KI is explained based on reference [15]. A continuous field variable $u(\mathbf{x})$ is defined in a domain Ω represented by a set of nodes $\mathbf{x}_i, i = 1, 2, \ldots, N$. Consider a point $\mathbf{x}_0$ in the domain, the estimation value of $u(\mathbf{x}_0)$ can be obtained using KI. The value of $u(\mathbf{x}_0)$ estimated by KI is represented by $u^h(\mathbf{x}_0)$, a linear combination of $u(\mathbf{x}_1), \ldots, u(\mathbf{x}_n)$, as described in Equation 17.

$$u^h(\mathbf{x}_0) = \sum_{i=1}^{n} \lambda_i \, u(\mathbf{x}_i) \tag{17}$$

where λ_i are the Kriging weights and n is the total number of nodes in the DOI of point $\mathbf{x}_0$. The functions $u(\mathbf{x}_1), \ldots, u(\mathbf{x}_n)$ are considered as realizations of random variables $U(\mathbf{x}_1), \ldots, U(\mathbf{x}_n)$. As a result, Equation 17 can be written as Equation 18.

$$U^h(\mathbf{x}_0) = \sum_{i=1}^{n} \lambda_i \, U(\mathbf{x}_i) \tag{18}$$

The Kriging weights are determined by making the $U^h(\mathbf{x}_0)$ unbiased by Equation 19.

$$E[U^h(\mathbf{x}_0) - U(\mathbf{x}_0)] = 0 \tag{19}$$

Moreover, the variance of the estimation error, viz (Equation 20).

$$\mathrm{var}[U^h(\mathbf{x}_0) - U(\mathbf{x}_0)] \tag{20}$$

is required to be minimized.

Using the Lagrange interpolation, the Kriging interpolation system can be obtained into Equations 21-22.

$$\mathbf{R\lambda} + \mathbf{P\mu} = \mathbf{r}(\mathbf{x}_0) \tag{21}$$

$$\mathbf{P^T\lambda} = \mathbf{p}(\mathbf{x}_0) \tag{22}$$

where $\mathbf{R}$ is an $n \, x \, n$ matrix of covariances and $\mathbf{P}$ is an $n \, x \, m$ matrix of polynomial values at the nodes. $\boldsymbol{\lambda}$ is an $n \, x \, 1$ vector of Kriging weights and $\boldsymbol{\mu}$ is an $m \, x \, 1$ vector of Lagrange multipliers. Furthermore, $\mathbf{r}(\mathbf{x}_0)$ is an $n \, x \, 1$ vector of covariance between the point $\mathbf{x}_0$ and the surrounding nodes. $\mathbf{p}(\mathbf{x}_0)$ is an $m \, x \, 1$ vector of polynomial basis at $\mathbf{x}_0$. A more detailed explanation can be found in Wong and Kanok-Nukulchai [15].

Using Equations 21-22, the Kriging weights can be obtained into Equations 23-25.

$$\boldsymbol{\lambda}^T = \mathbf{p}^T(\mathbf{x}_0)\mathbf{A} + \mathbf{r}^T(\mathbf{x}_0)\mathbf{B} \tag{23}$$

$$\mathbf{A} = (\mathbf{P}^T\mathbf{R}^{-1}\mathbf{P})^{-1}\mathbf{P}^T\mathbf{R}^{-1} \tag{24}$$

$$\mathbf{B} = \mathbf{R}^{-1}(\mathbf{I} - \mathbf{PA}) \tag{25}$$

where $\mathbf{I}$ is an $n \, x \, n$ identity matrix. Therefore, Equation 17 can be written into Equations 26-27.

$$u^h(\mathbf{x}_0) = \boldsymbol{\lambda}^T\mathbf{d} \tag{26}$$

$$\mathbf{d} = [u(\mathbf{x}_1) \quad \ldots \quad u(\mathbf{x}_n)]^T \tag{27}$$

where $\mathbf{d}$ is an $n \, x \, 1$ vector of nodal values. Changing the symbol $\mathbf{x}_0$ by $\mathbf{x}$, Equation 26 can be written into Equation 28.

$$u^h(\mathbf{x}) = \mathbf{N}(\mathbf{x})\mathbf{d} = \sum_{i=1}^{n} N_i(x)u_i \tag{28}$$

Here, $\mathbf{N}(\mathbf{x})$ is the matrix of shape functions. For constructing the Kriging shape functions, the polynomial basis function and the covariance function are needed. The complete and incomplete polynomial bases can be used as the polynomial basis function. On the other hand, the correlation function is defined by Equations 29-30.

$$\rho(\mathbf{h}) = \frac{C(\mathbf{h})}{\sigma^2} \tag{29}$$

$$\sigma^2 = \mathrm{var}[U(\mathbf{x})] \tag{30}$$

where $\rho(\mathbf{h})$ is the correlation function and $\mathbf{h}$ is a vector separating the points $\mathbf{x}$ and $\mathbf{x} + \mathbf{h}$. In this research, the value of σ^2 was taken as 1. Moreover, the quartic spline (QS) correlation function was used. The QS correlation function for $0 \le \theta\frac{h}{d} \le 1$ is described by Equation 31.

$$\rho(\mathbf{h}) = 1 - 6\left(\theta\frac{h}{d}\right)^2 + 8\left(\theta\frac{h}{d}\right)^3 - 3\left(\theta\frac{h}{d}\right)^4 \tag{31}$$

For $\theta\frac{h}{d} > 1$, the QS correlation function is defined as 0. Here, h is defined as the Euclidean distance between the points $\mathbf{x}$ and $\mathbf{x}+\mathbf{h}$, d is the maximum distance between points in the DOI and θ is known as the correlation parameter. The QS correlation parameter function for $n \geq 10$ is 1. For $3 \leq n < 10$, the value of θ is defined by Equation 32.

$$\theta = 0.1329n - 0.3290 \qquad (32)$$

Based on the previous research [15], it was found that there is a minimum number of layers for an m-order polynomial basis function. The minimum number of layers for linear, quadratic, and cubic polynomial basis functions are one, two, and three, respectively. The linear polynomial basis function with one layer of elements is the same as the conventional FEM.

4 Numerical examples

Two-dimensional linear elasticity problems of a hollow cylinder and an infinite plate with a central hole [19] were considered. Fig. 4 shows a plane stress problem of a hollow cylinder under internal pressure. Due to the symmetry, only one-quarter of the problem domain was analyzed. Pin supports are located along the sides $x = 0$ and $y = 0$. The geometrical and material parameters of the problem are a = 1.0, b = 5.0, p = 1.0, E = 1.0 x 10^3, and v = 0.25. Any consistent unit can be used.

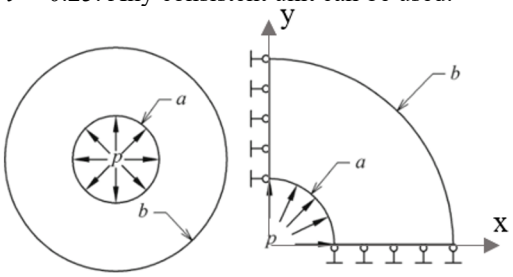

Fig. 4. A hollow cylinder under internal pressure [19].

Fig. 5 shows a plane strain problem of an infinite plate with a central hole. Due to symmetry, only one-quarter of the problem was modeled. The geometrical and material parameters are a = 1.0, b = 5.0, P = 1.0, E = 1.0 x 10^3, and v = 0.25. Analytical surface tractions are applied along the sides x = 5 and y = 5. Pin supports are also located along the sides x = 0 and y = 0. Any consistent unit can be used.

In this research, all computations of stiffness matrices and nodal forces used six Gauss sampling points. However, for calculating the element errors using the EFG error indicator, two different numbers of Gauss sampling points were used ($m_g = 6$ and $n_g = 1$).

To run the AMR procedure, the initial mesh was first determined. Afterward, the point, edge, triangle, geometry, and boundary condition matrices were exported to the main workspace as the input data of the program. The value of $\beta_{\varepsilon,\mathrm{tol}}$ and the limit of RSED were also determined based on the criteria described above. The results presented for each problem are the final mesh configurations obtained with the K-FEM using linear, quadratic, and cubic polynomial basis functions. One and two layers of elements, two and three layers of elements, and three layers of elements were used for linear, quadratic, and cubic polynomial basis functions, respectively.

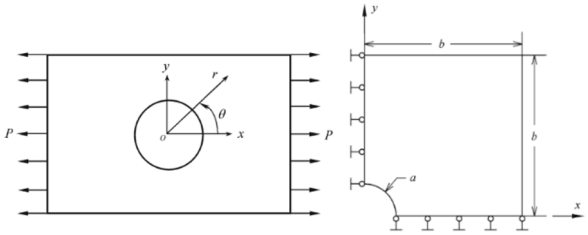

Fig. 5. An infinite plate with a central hole [19].

4.1 Hollow cylinder

The initial mesh with 40 elements, shown in Fig. 6, was used for this problem. The value of $\beta_{\varepsilon,\mathrm{tol}}$ was 0.25 and the limit of RSED was 0.05. Moreover, the exact total strain energy (U_{ex}) was 0.00105.

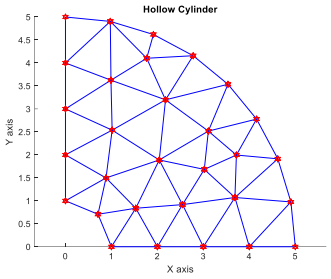

Fig. 6. Initial mesh of the hollow cylinder problem.

4.1.1 SER error indicator

The final meshes for the linear, quadratic, and cubic polynomial basis functions presented are shown in Fig. 7-9.

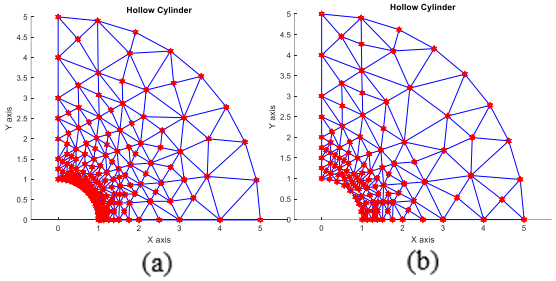

Fig. 7. The final mesh configurations of the hollow cylinder problem obtained using the SER error indicator for a linear polynomial basis function with (a) one and (b) two layers of elements.

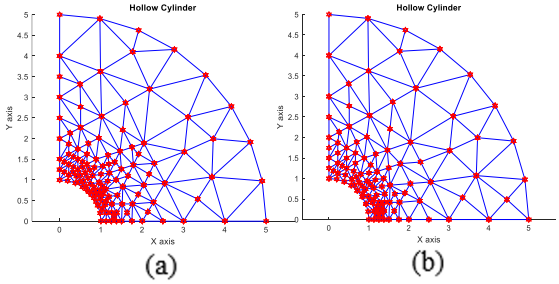

Fig. 8. The final mesh configurations of the hollow cylinder problem obtained using the SER error indicator for a quadratic polynomial basis function with (a) two and (b) three layers of elements.

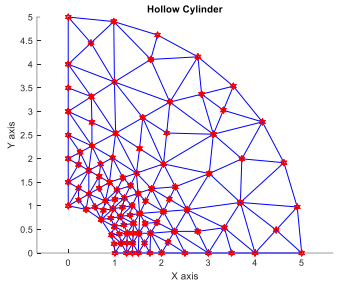

Fig. 9. The final mesh configuration of the hollow cylinder problem obtained using the SER error indicator for a cubic polynomial basis function with three layers of elements.

4.1.2 GES error indicator

The final mesh configurations for linear, quadratic, and cubic polynomial basis functions are shown in Fig. 10-12.

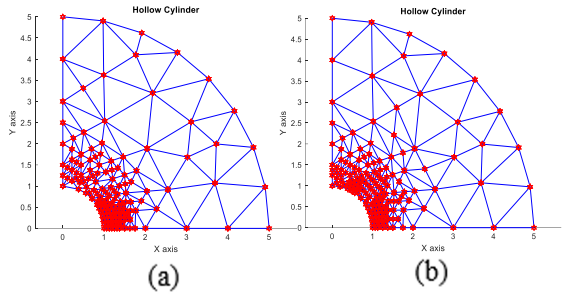

Fig. 10. The final mesh configurations of the hollow cylinder problem obtained using the GES error indicator for a linear polynomial basis function with (a) one and (b) two layers of elements.

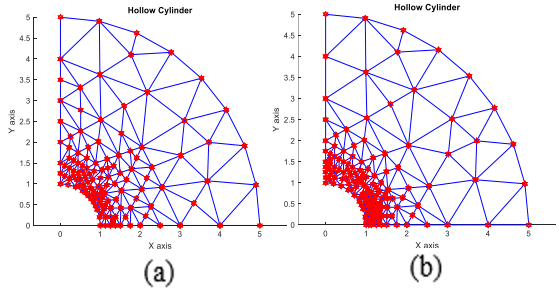

Fig. 11. The final mesh configurations of the hollow cylinder problem obtained using the GES error indicator for a quadratic polynomial basis function with (a) two and (b) three layers of elements.

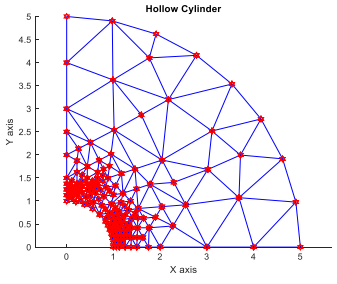

Fig. 12. The final mesh configuration of the hollow cylinder problem obtained using the GES error indicator for a cubic polynomial basis function with three layers of elements.

4.1.3 EFG error indicator

The final meshes for the linear, quadratic, and cubic polynomial basis functions presented are shown in Fig. 13-15.

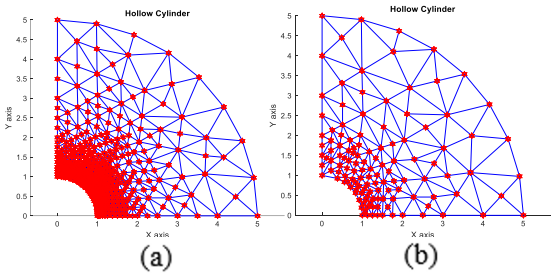

Fig. 13. The final mesh configurations of the hollow cylinder problem obtained using the EFG error indicator for a linear polynomial basis function with (a) one and (b) two layers of elements.

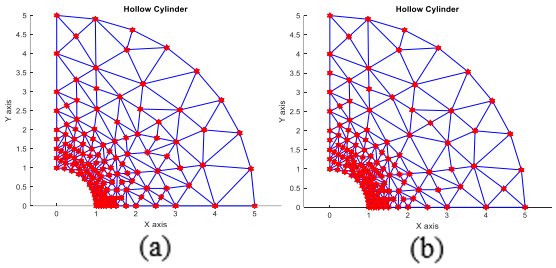

Fig. 14. The final mesh configurations of the hollow cylinder problem obtained using the EFG error indicator for a quadratic polynomial basis function with (a) two and (b) three layers of elements.

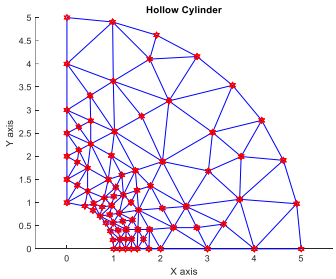

Fig. 15. The final mesh configuration of the hollow cylinder problem obtained using the EFG error indicator for a cubic polynomial basis function with three layers of elements.

4.1.4 Discussion

Table 1 shows the total number of elements, RSER, and RSED of the linear, quadratic, and cubic polynomial bases for the final mesh configurations obtained using the SER, GES, and EFG error indicators.

In general, the most effective error indicator can be found based on its ability to detect areas with stress concentration. This is done by considering the final mesh configurations generated with each error indicator. Moreover, the total number of elements, the value of RSER, and the value of RSED may also be considered as the criteria for determining the most effective error indicator. However, those values based on the total strain energy may not be the most reliable criteria because of several factors that can influence the results. One of the factors affecting the results is the element distribution. The RSED value may not also be the most reliable criterion as it depends on the difference between the total strain energy of the current and previous iterations. In addition, the most effective error indicator must be independent of the type of problems being analyzed. This means, for all problems, the most effective error indicator must have the capability to properly detect elements that must be refined.

Table 1. Total number of elements, RSER, and RSED of final mesh configurations for the hollow cylinder problem using the SER, GES, and EFG error indicators.

Error Indicator	Linear (1 Layer)		
	Elements	RSER	RSED
SER	293	0.02190	0.01666
GES	266	0.04173	0.04902
EFG	985	0.01570	0.00428
Error Indicator	Linear (2 Layers)		
	Elements	RSER	RSED
SER	207	0.02553	0.03208
GES	294	0.04319	0.02204
EFG	219	0.03502	0.02687
Error Indicator	Quadratic (2 Layers)		
	Elements	RSER	RSED
SER	221	0.00882	0.02602
GES	300	0.04143	0.03101
EFG	253	0.04891	0.02218
Error Indicator	Quadratic (3 Layers)		
	Elements	RSER	RSED
SER	190	0.02053	0.03380
GES	269	0.03883	0.01771
EFG	266	0.04852	0.01654
Error Indicator	Cubic (3 Layers)		
	Elements	RSER	RSED
SER	170	0.01793	0.00737
GES	292	0.04431	0.01193
EFG	132	0.12124	0.03231

For the conventional FEM, based on the total number of elements, RSER, and RSED, it could be observed that the SER indicator might be the most effective error indicator. However, the refinement process tended to distribute throughout the problem domain. This behavior could be observed more clearly on the final mesh configuration for the cubic polynomial basis function. On the other hand, considering the values of RSER and RSED, the GES error indicator could be viewed as the second most effective error indicator for almost all polynomial basis functions. Nevertheless, based on the final mesh configurations, this error indicator appeared to perform well for all polynomial basis functions, especially for the quadratic and cubic polynomial basis functions. Unlike the SER error indicator, the AMR procedure tended to be consistently concentrated around the inner radius corner. Furthermore, the EFG error indicator tended to give the lowest value of RSER for the conventional FEM. However, in this case, this error indicator generated the largest number of elements. This was because this error indicator is based on the element strain energy error. In the conventional FEM, the stress within the element is constant throughout the element. As a result, the difference between the strain energy errors calculated using a different number of Gauss integration points is certainly very small. Therefore, the effectiveness of this error indicator is low. Nevertheless, as the order of the polynomial basis functions increased, this error indicator tended to perform better.

From the results, it was also found that initial mesh configurations, refinement criteria, and termination criteria affected the total number of elements. The authors tried to use a different initial mesh with 68 elements. Fig. 16 shows the initial (68 elements) and final (457 elements) mesh configurations for the conventional FEM using the GES error indicator. It can be seen that finer meshes tend to generate more elements. In addition, the AMR can be distributed more evenly around the inner radius corner in comparison to the results obtained with 40 elements.

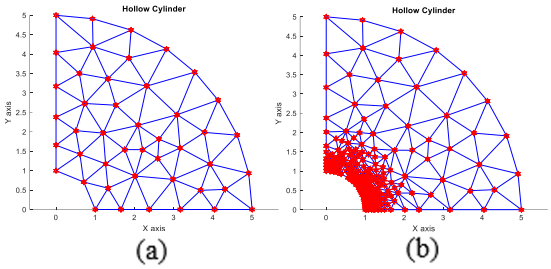

Fig. 16. The (a) initial (68 elements) and (b) final (457 elements) meshes for the conventional FEM.

Furthermore, the mesh configuration could influence the effectiveness of the K-FEM itself. The K-FEM tends to work more effectively for a uniform mesh configuration. A significant difference in distances between nodes can reduce the effectiveness of the K-FEM as it will affect the correlation matrix. Moreover, the K-FEM is nonconforming (incompatible) [15]. The KI is not perfectly continuous along the edges of the elements. This is because the KI of two adjacent elements can be formed by a different set of nodes. For a particular mesh configuration, the degree of error may be influenced by the degree of incompatibility. In consequence, as observed in this research, the total number of elements for the K-FEM with a quadratic polynomial basis function could be larger than the one with a linear polynomial basis function.

The total number of elements could also be affected by the refinement criterion ($\beta_{\varepsilon,\mathrm{tol}}$). The lower the value of $\beta_{\varepsilon,\mathrm{tol}}$, the more the elements chosen to be refined. Similarly, the lower the limit of RSED, the higher the total number of elements could be.

4.2 Infinite plate with a central hole

Fig. 17 shows the initial mesh consisted of 40 elements. The value of $\beta_{\varepsilon,\mathrm{tol}}$ was 0.55 and the limit of RSED was 0.003. Moreover, the exact total strain energy (U_{ex}) was 0.01217.

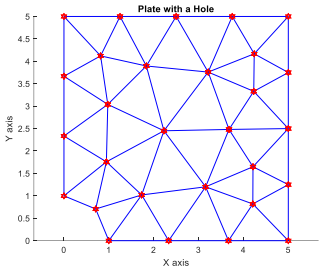

Fig. 17. Initial mesh of the infinite plate with a central hole problem.

4.2.1 SER error indicator

The final meshes for the linear, quadratic, and cubic polynomial basis functions presented are shown in Fig. 18-20.

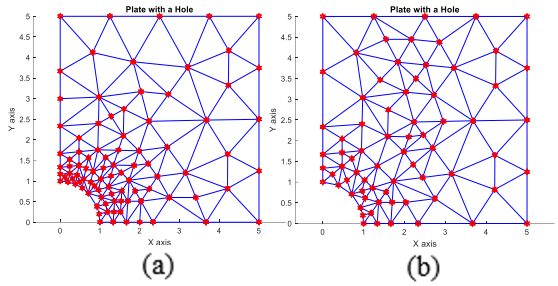

Fig. 18. The final mesh configurations of the infinite plate with a central hole problem obtained using the SER error indicator for a linear polynomial basis function with (a) one and (b) two layers of elements.

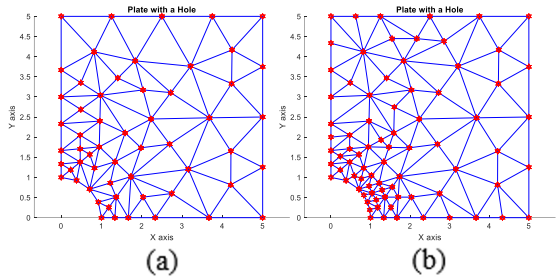

Fig. 19. The final mesh configurations of the infinite plate with a central hole problem obtained using the SER error indicator for a quadratic polynomial basis function with (a) two and (b) three layers of elements.

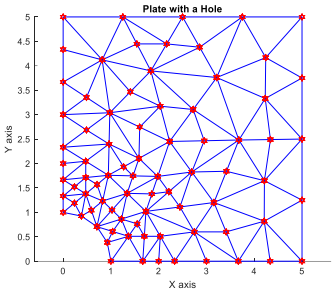

Fig. 20. The final mesh configuration of the infinite plate with a central hole problem obtained using the SER error indicator for a cubic polynomial basis function with three layers of elements.

4.2.2 GES error indicator

The final mesh configurations for linear, quadratic, and cubic polynomial basis functions are shown in Fig. 21-23.

4.2.3 EFG error indicator

The final meshes for the linear, quadratic, and cubic polynomial basis functions are shown in Fig. 24-26.

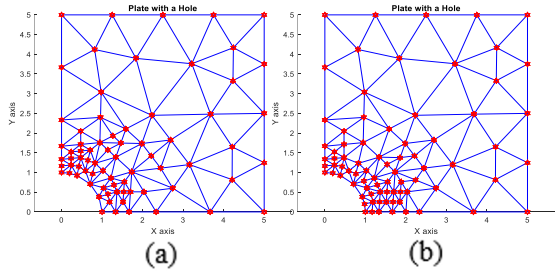

Fig. 21. The final mesh configurations of the infinite plate with a central hole problem obtained using the GES error indicator for a linear polynomial basis function with (a) one and (b) two layers of elements.

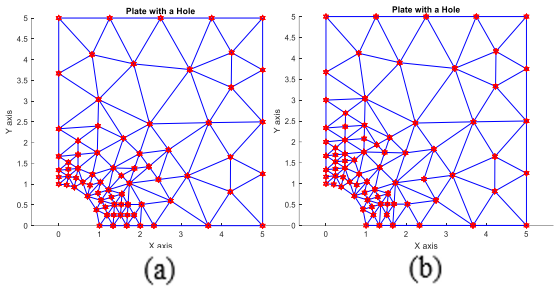

Fig. 22. The final mesh configurations of the infinite plate with a central hole problem obtained using the GES error indicator for a quadratic polynomial basis function with (a) two and (b) three layers of elements.

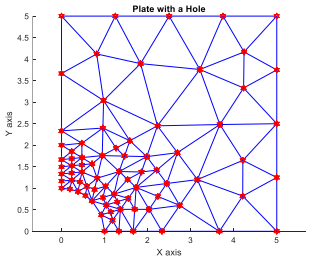

Fig. 23. The final mesh configuration of the infinite plate with a central hole problem obtained using the GES error indicator for a cubic polynomial basis function with three layers of elements.

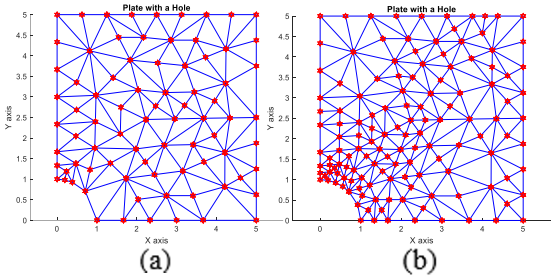

Fig. 24. The final mesh configurations of the infinite plate with a central hole problem obtained using the EFG error indicator for a linear polynomial basis function with (a) one and (b) two layers of elements.

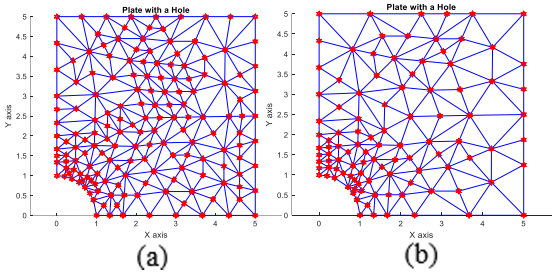

Fig. 25. The final mesh configurations of the infinite plate with a central hole problem obtained using the EFG error indicator for a quadratic polynomial basis function with (a) two and (b) three layers of elements.

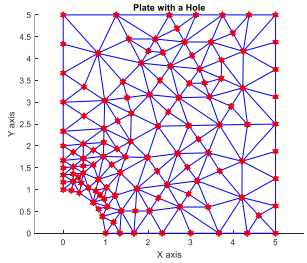

Fig. 26. The final mesh configuration of the infinite plate with a central hole problem obtained using the EFG error indicator for a cubic polynomial basis function with three layers of elements.

4.2.4 Discussion

The total number of elements, RSER, and RSED of the linear, quadratic, and cubic polynomial basis functions for the final mesh configurations obtained with the SER, GES, and EFG error indicators are shown in Table 2.

Table 2. Total number of elements, RSER, and RSED of final mesh configurations for the infinite plate with a central hole problem using the SER, GES, and EFG error indicators.

Error Indicator	Linear (1 Layer)		
	Elements	**RSER**	**RSED**
SER	154	0.00495	0.00245
GES	120	0.00765	0.00232
EFG	127	0.01377	0.00225
Error Indicator	**Linear (2 Layers)**		
	Elements	**RSER**	**RSED**
SER	119	0.00207	0.00260
GES	129	0.00019	0.00287
EFG	231	0.00002	0.00124
Error Indicator	**Quadratic (2 Layers)**		
	Elements	**RSER**	**RSED**
SER	89	0.00216	0.00189
GES	121	0.00033	0.00278
EFG	286	0.00269	0.00271
Error Indicator	**Quadratic (3 Layers)**		
	Elements	**RSER**	**RSED**
SER	164	0.00169	0.00267
GES	128	0.00161	0.00177
EFG	174	0.00221	0.00217
Error Indicator	**Cubic (3 Layers)**		
	Elements	**RSER**	**RSED**
SER	129	0.00450	0.00278
GES	127	0.00032	0.00296
EFG	205	0.00207	0.00195

In this problem, the behavior of each error indicator could be observed more clearly. The higher the order of the polynomial basis, the lower the effectiveness of the SER error indicator. This behavior could be seen particularly in the final mesh configurations for the quadratic and cubic polynomial basis functions with three layers of elements. The AMR was not only concentrated around the hole but also distributed throughout the whole domain. This behavior was observed because the SER error indicator is based on the averaged (smoothed) stress. Theoretically, the SER error indicator will work more effectively for the linear polynomial basis function with one layer of elements (conventional FEM). The stress field occurring in the conventional FEM is not continuous along the element edges between two neighboring elements. As a result, the difference between the averaged and unaveraged stresses is large. Hence, the SER tends to work more effectively for the conventional FEM.

On the other hand, similar to the previous problem, the GES error indicator worked effectively for all polynomial basis functions. It could also be observed that the value of RSER and the total number of elements for the GES error indicator were mostly the lowest compared to the other error indicators. The authors also tried to plot the stress around the corner of the hole. Based on the stress plot, the stress concentration at the corner of the hole could be captured quite well.

Moreover, the EFG error indicator worked ineffectively based on the final mesh configurations, especially for the linear and quadratic polynomial basis functions. The area around the hole shown in the final mesh configuration of the conventional FEM was not even accurately refined. However, as the order of the polynomial basis increased, this error indicator could perform better. This could be observed from the value of RSER which tended to get lower.

5 Conclusions

The effectiveness of each error indicator in the AMR can be observed through several criteria. Several criteria considered are the total number of elements, the values of RSER and RSED, the final mesh configurations, and the independence from the type of problems being analyzed. Nevertheless, in some cases, a large total number of elements and a high value of RSER are not always an indication that the error indicator used is less effective than the others. The reason for this is that even though there may be a large number of elements and a high value of RSER, the AMR procedure may instead be more concentrated in the area with stress concentration. Based on this observation, it can be concluded that the GES indicator is the most effective error indicator as it can accurately estimate the element errors and work effectively for the K-FEM with all polynomial basis functions for each problem presented.

Moreover, the effectiveness of the K-FEM can be affected by several factors, such as the initial mesh configurations, the refinement criteria, and the termination criteria. Therefore, these factors must always be considered in the AMR procedure for the K-FEM analyses.

References

1. G.R. Liu, Meshfree methods: moving beyond the finite element method 2nd ed. (CRC Press, Boca Raton, 2009)
2. R.D. Cook, Finite element modeling for stress analysis (John Wiley & Sons, Inc., Canada, 1995)
3. O.C. Zienkiewicz, J.Z. Zhu, International Journal for Numerical Methods in Engineering **24**(2), 337-357 (1987) https://doi.org/10.1002/nme.1620240206
4. M.X.D. Li, R. Moshfegh, L. Nilsson, Communications in Numerical Methods in Engineering **16**(11), 785-800 (2000) https://doi.org/10.1002/1099-0887(200011)16:11%3C785::AID-CNM376%3E3.0.CO;2-8
5. R. Moshfegh, X. Li, L. Nilsson, Engineering Computations **17**(8), 910-932 (2000) https://doi.org/10.1108/02644400010360875
6. P. Pudjisuryadi, Civil Engineering Dimension **10**(2), 99-108 (2008) https://doi.org/10.9744/ced.10.2.pp.%2099-108

7. G.R. Liu, Z.H. Tu, Computer Methods in Applied Mechanics and Engineering **191**(17-18), 1923-1943 (2002) https://doi.org/10.1016/S0045-7825(01)00360-7
8. J.Z. Zhu, O.C. Zienkiewicz, International Journal for Numerical Methods in Engineering **30**(7), 1321-1339 (1990) https://doi.org/10.1002/nme.1620300707
9. O.C. Zienkiewicz, J.Z. Zhu, International Journal for Numerical Methods in Engineering **33**(7), 1365-1382 (1992) https://doi.org/10.1002/nme.1620330703
10. C.K. Lee, S.H. Lo, Engineering Fracture Mechanics **50**(5-6), 671-686 (1995) https://doi.org/10.1016/0013-7944(94)E0053-J
11. A. Tabarraei, N. Sukumar, Finite Elements in Analysis and Design **41**(7-8), 686-702 (2005) https://doi.org/10.1016/j.finel.2004.08.002
12. S.W. Kwang, J.S. Ahn, Mathematical Problems in Engineering 1790256 (2017) https://doi.org/10.1155/2017/1790256
13. O.C. Zienkiewicz, R.L. Taylor, J.Z. Zhu, The finite element method: Its basis and fundamentals. 6th ed. (Elsevier Butterworth-Heinemann, Oxford, 2005)
14. K. Plengkhom, W. Kanok-Nukulchai, International Journal of Computational Methods **2**(4), 451-475 (2005) https://doi.org/10.1142/S0219876205000594
15. F.T. Wong, W. Kanok-Nukulchai, International Journal of Computational Methods **6**(1), 93-118 (2009) https://doi.org/10.1142/S0219876209001784
16. F.T. Wong, W. Kanok-Nukulchai, Civil Engineering Dimension **11**(1), 15-22 (2009) https://doi.org/10.9744/ced.11.1.pp.%2015-22
17. K-N. Worsak, F.T. Wong, W. Sommanawat, Civil Engineering Dimension **17**(3), 152-157 (2015) https://doi.org/10.9744/ced.17.3.152-157
18. Z. Masood, Thesis, Asian Institute of Technology (2006) http://203.159.12.58/ait-thesis/detail.php?id=B10057
19. C. Zheng, S.C. Wu, X.H. Tang, J.H. Zhang, Acta Mech Sin **26**, 265-278 (2010) https://doi.org/10.1007/s10409-009-0265-3
20. MathWorks, Partial differential equation toolbox: For use with MATLAB: Computer solutions Europe AB (The MathWorks, Inc., Natick, 1996)
21. K.H. Muci-Kiichler, J.C. Miranda-Valenzuela, WIT Transactions on Modelling and Simulation **16**, 351-360 (1997) DOI: 10.2495/BT970331
22. L. Gu, International Journal for Numerical Methods in Engineering **56**(1), 1-11 (2003) https://doi.org/10.1002/nme.553